Impedance spectroscopy of multiferroic $PbZr_xTi_{1-x}O_3/CoFe_2O_4$ layered thin films

N. Ortega,[1] Ashok Kumar,[1] P. Bhattacharya,[2] S. B. Majumder,[3] and R. S. Katiyar[1,*]

[1]*Department of Physics and Institute for Functional Nanomaterials, University of Puerto Rico, San Juan, Puerto Rico 00931-3343, USA*

[2]*Department of Physics, Fisk University, Nashville, Tennessee 37208, USA*

[3]*Materials Science Center, Indian Institute of Technology, Kharagpur 721302, India*

(Received 9 July 2007; revised manuscript received 10 October 2007; published 28 January 2008)

The electrical properties of ferroelectric $Pb(Zr,Ti)O_3$ (PZT) and ferromagnetic $CoFe_2O_4$ (CFO) thin film multilayers (MLs) fabricated by pulsed laser deposition technique has been studied by impedance and modulus spectroscopy. The effect of various PZT/CFO configurations having three, five, and nine layers has been systematically investigated. The transmission electron microscopy images revealed that the ML structures were at least partially diffused near the interface. Diffraction patterns indicate clear PZT and CFO crystal structures in the interior and at the interface of the ML structure. Room temperature micro-Raman spectra indicate separate PZT and CFO phases in ML structure without any impurity phase. We studied frequency and temperature dependencies of impedance, electric modulus, and ac conductivity of ML thin films in the ranges of 100 Hz–1 MHz and 200–650 K, respectively. We observed two distinct electrical responses in all the investigated ML films at low temperature (<400 K) and at elevated temperature (>400 K). We attributed these contributions to the grain effects at low temperature and grain boundary effects at high temperature. We explained this electrical behavior by Maxwell-Wagner-type contributions arising from the interfacial charge at the interface of the ML structure. Master modulus spectra indicate that the magnitude of grain boundary compared to grain becomes more prominent with the increase in the number of layer. The frequency dependent conductivity results well fitted with the double power law, $\sigma(\omega)=\sigma(0)+A_1\omega^{n1}+A_2\omega^{n2}$, and the results showed evidence of three types of conduction process at elevated temperature: (i) low frequency (<1 kHz) conductivity is due to long-range ordering (frequency independent), (ii) midfrequency conductivity (<10 kHz) may be due to the short-range hopping, and (iii) high frequency (<1 MHz) conduction is due to the localized relaxation hopping mechanism.

DOI: 10.1103/PhysRevB.77.014111 PACS number(s): 68.37.Lp, 73.50.−h, 73.40.−c, 74.78.Fk

I. INTRODUCTION

Recently, considerable attention has been focused on multiferroic materials due to their multifunctionality that could lead to potential applications in highly sensitive sensors and actuators as well as multistate memory devices.[1] Their magnetic as well as electrical polarization ordering and the coupling between these two order parameters characterized these multiferroic materials.[2] Several efforts have been made to synthesize magnetoelectric (ME) composite thin films with coexisting ferroelectric (FE) and ferromagnetic (FM) properties for the next generation miniaturized integrated devices. Different configurations were reported for the fabrication of ME composite thin films, such as composite spreads with terminal layers being FE and FM,[3] double $Pb(Zr,Ti)O_3$(PZT)/$CoFe_2O_4$(CFO) multilayers,[4] superlattices consisting of alternating FM ($Pr_{0.88}Ca_{0.15}MnO_3$) and FE ($Ba_{0.6}Sr_{0.4}TiO_3$) layers deposited on $SrTiO_3$,[5] epitaxial $CoFe_2O_4$-$BaTiO_3$ ferroelectromagnetic nanocomposites by self-assembly technique,[6] etc. These studies clearly demonstrated the ME effect in all different configurations. Recently, we have reported that the PZT/CFO multilayer composite thin films exhibited ME effect.[7] Complex impedance spectroscopy is a powerful and versatile technique to analyze the microstructure-property relationship, and it also allows distinguishing between intrinsic (bulk) and extrinsic contributions (grain boundary, surface layer, and electrode contact problem). An equivalent circuit based on impedance and modulus spectra provides the physical process occurring inside the sample. Impedance spectroscopy studies of ferroelectromagnetic ceramic $Pb(Fe_{1/2}Nb_{1/2})O_3$ and magnetoelectric polycrystalline samples $Bi_6Fe_2Ti_3O_{12}$ has been carried out; they described the connection between microstructure and electrical properties in terms of the brick-layer model[8] and parallel resistance (R)–capacitance (C) circuit.[9] The electrical and dielectric behaviors of $CaCu_3Ti_4O_{12}$,[10] $Bi_{2/3}Cu_3Ti_4O_{12}$,[11] and $ACu_3Ti_4O_{12}$ (A=Ca, $Bi_{2/3}$, $Y_{2/3}$, $La_{2/3}$) (Ref. 12) ceramic samples and ZrTiO4 thin films[13] are discussed with the help of impedance spectroscopy. They all exhibit a Debye-like relaxation (Maxwell-Wagner type) and their dielectric constant is nearly independent of frequency and temperature. Catalan *et al.* did an extensive study on the Maxwell-Wagner space charge effects in a superlattice structure.[14,15] Recently, we have observed the Maxwell-Wagner charge effects in the PZT-CFO multilayer (ML) structure.[16] However, impedance analysis of ME multilayer thin films has not been reported so far. Our results indicate similar behavior of electrical and dielectric properties, as reported for giant dielectric constant materials having grain boundary effects.[10–12]

We studied the impedance, modulus, and ac conductivity of the ML structure as a function of the temperature (200–650 K) and frequency (10^2–10^6 Hz). The goal of this investigation is to improve our understanding of the PZT/CFO ML thin film properties by analyzing the electrical response of the grain and grain boundary effects, making an interpretation of the microscopic process that allows discerning the roll of PZT and CFO interface in the conductivity

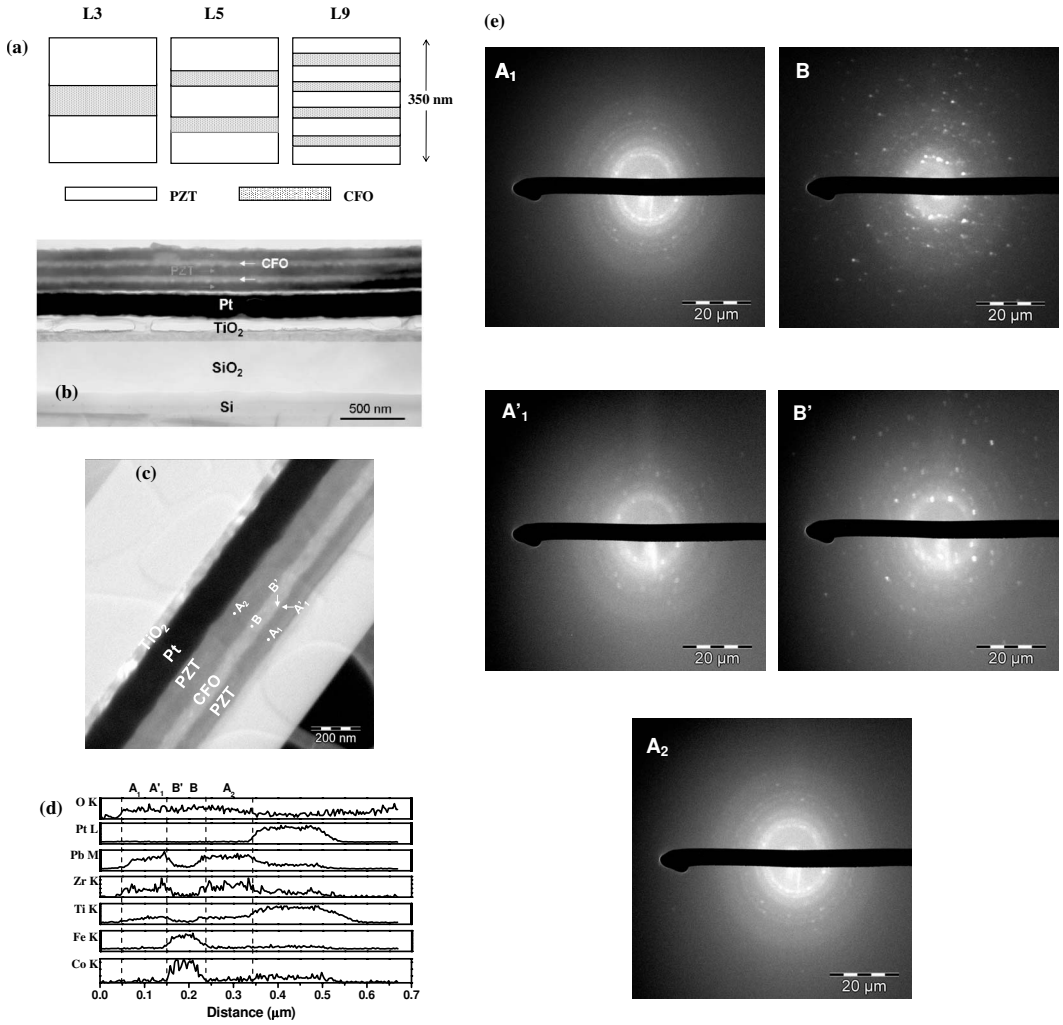

FIG. 1. (a) Schematic structures of multilayer PZT/CFO thin films. Cross-sectional low magnification TEM image of the PZT/CFO. (b) Five-layer and (c) three-layer thin films. (d) STEM line scale of L3 ML structure and (e) diffraction patterns of PZT upper layer (A_1), CFO (B), PZT lower layer (A_2), A'_1 (toward PZT), and B' (toward CFO) at the interface.

process in the different configurations of the PZT-CFO ML structures. In the present work, we have synthesized three, five, and nine ML structures with alternating PZT and CFO layers on platinized silicon using pulsed laser deposition technique in order to investigate the effect of the distribution of FE and FM phases and the influence of interface layers on the electrical properties of ML structures.

II. EXPERIMENT

Multilayer thin films with three (L3), five (L5), and nine (L9) alternating layers of PZT/CFO were deposited from individual PZT and CFO targets on $Pt/TiO_2/SiO_2/Si$ substrates using pulsed laser deposition technique [see Fig. 1(a)]. The PZT and CFO ceramic targets of 2 cm diameter were prepared by the conventional solid-state route. An excimer laser (KrF, 248 nm) with a laser energy density of 2.5 J/cm^2 and pulse repetition rate of 10 Hz was used to deposit the ML films. During the deposition, the substrate temperature was maintained at 400 °C and oxygen pressure of 100 mTorr. The deposited films were annealed at 650 °C for 150 s using a rapid thermal annealing furnace. The total thickness of all the films was ~350 nm in these deposition parameters. The high-resolution transition electron microscope (TEM) was used to investigate the formation of ML PZT/CFO structures and the interdifussion of constituent PZT and CFO layers. For electrical measurement, the capacitors were fabricated by sputtering Pt top electrodes with a diameter of ~200 μm through a shadow mask. The impedance $|Z|$ and phase angle (θ) were measured in the frequency range from 10^2 to 10^6 Hz using an HP4294 impedance analyzer. The temperature dependence impedance measurements were carried out at an interval of 20 K in the range from 200 to 650 K and the temperature was controlled with an accuracy of ±0.6 °C using a temperature controller (K-20 MMR technologies, Inc.).

III. DATA ANALYSIS

The real (Z') and imaginary (Z'') parts of the complex impedance (Z^*) were obtained using the relations

$$Z' = Z \cos \theta, \tag{1}$$

$$Z'' = Z \sin \theta. \quad (2)$$

For electrical modulus data analysis, the complex impedance can be converted to the complex modulus

$$M^* = i\omega C_0 Z^* = i\omega C_0 (Z' - iZ'') = M' + iM'', \quad (3)$$

via

$$M' = \omega C_0 Z'' \text{ and } M'' = \omega C_0 Z'. \quad (4)$$

$C_0 = \varepsilon_0 A/d$ is the vacuum capacitance of the measuring cell and electrodes with an air gap of the sample thickness, where ε_0 is the permittivity of free space (8.854×10^{-12} F/m), d is the sample thickness, and A is the cross-sectional area of the electrode deposited on the sample; ω is the angular frequency.

The ac conductivity σ_{ac} was calculated using the relation

$$\sigma_{ac} = \frac{d \sin \theta}{A|Z|}. \quad (5)$$

IV. RESULTS AND DISCUSSION

A. Multilayer structure analysis

The sketch diagram of different MLs, i.e., L3, L5, and L9 thin films, is shown in Fig. 1(a). We maintained equal thickness for all the MLs with a PZT to CFO thickness ratio of 60:40. This particular thickness has been carried out for the present investigation to maintain the FE and FM properties and their coupling. The cross-sectional TEM image of PZT-CFO with three and five layers are shown in Figs. 1(b) and 1(c). From Fig. 1(b), TEM reveals that the film thickness is uniform over a region of several nanometers and the formation of ML PZT-CFO structure is observed. TEM micrographs show the clear view of the PZT/CFO interface with little interdifussion of PZT into CFO and CFO into PZT layers forming an inhomogeneous structure at the interface; however, far from the interface, minor diffusion of the layers on either side is observed. TEM micrograph of L3 [Fig. 1(c)] indicates little interdiffusion at the interface; however, it increases with the increase in the number of layers of ML. The scanning transmission electron microscopy (STEM) across the ML structure is shown in Fig. 1(d), which indicates clear ML structure with little interdiffusion of the pure PZT and pure CFO at the interface. TEM has been used to see the diffraction patterns of the ML structure near the interface with spot size (~2–6 nm). We observed clear diffraction patterns of PZT and CFO at the center of each layer and either PZT or CFO diffraction patterns near the interface depend on the focus of electron beam toward PZT or CFO side. In Fig. 1(e), A_1, B, A_2, A_1', and B' represent the diffraction patterns of the PZT upper layer, CFO, PZT lower layer, PZT toward the PZT side near the interface, and CFO toward the CFO side near the interface. The observed diffraction patterns near the interface that either belong to PZT or CFO indicate the chemical purity near the interface. The PZT-CFO ML structure was further investigated using micro-Raman spectroscopy in order to verify the chemical impurity in the ML structure. There were no additional phases apart from

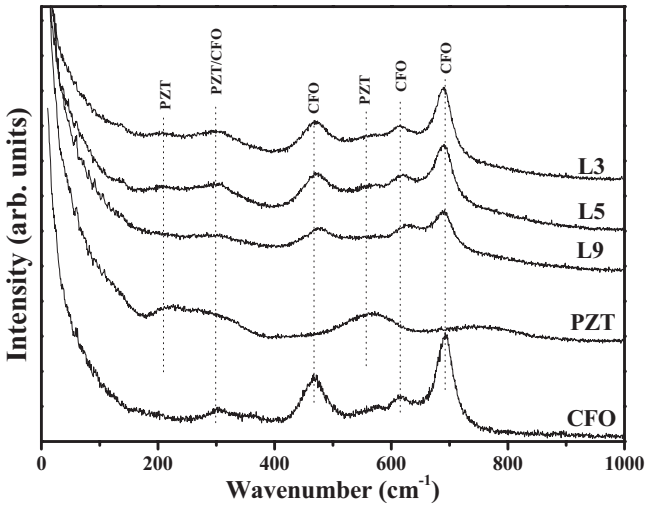

FIG. 2. Room temperature Raman spectra for CFO, PZT, and multilayer (L3, L5, and L9) thin films annealed at 650 °C.

PZT and CFO in the ML thin films. Figure 2 shows room temperature micro-Raman spectra of the CFO, PZT, and multilayer thin films, all the peaks of ML thin films can be assigned to the PZT or CFO structure, and there are no additional peaks that indicate no intermediate compounds in multilayer thin films. The observation of distinct phases for PZT and CFO in both x-ray[16] and Raman spectra for PZT-CFO films confirms that the films have two distinct phases after the annealing process.

The depth profiles of the constituent elements of PZT-CFO multilayers near the interface are described elsewhere.[7] STEM and depth profile data indicate that the as deposited ML structure was not maintained but partially diffused near the interface. In order to get a further understanding of the above experimental data to establish a connection between

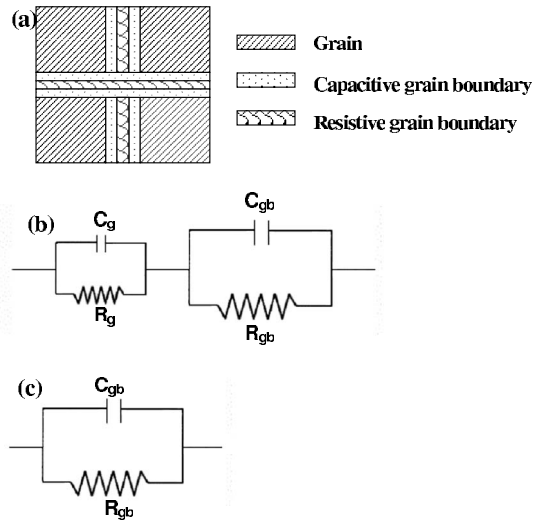

FIG. 3. (a) Microstructural model used here based on the brick-layer model. (b) Equivalent circuit used to represent the electrical properties of grain and grain boundary effects. (c) Equivalent circuit used to describe the electrical properties of ML at high temperatures (>400 K).

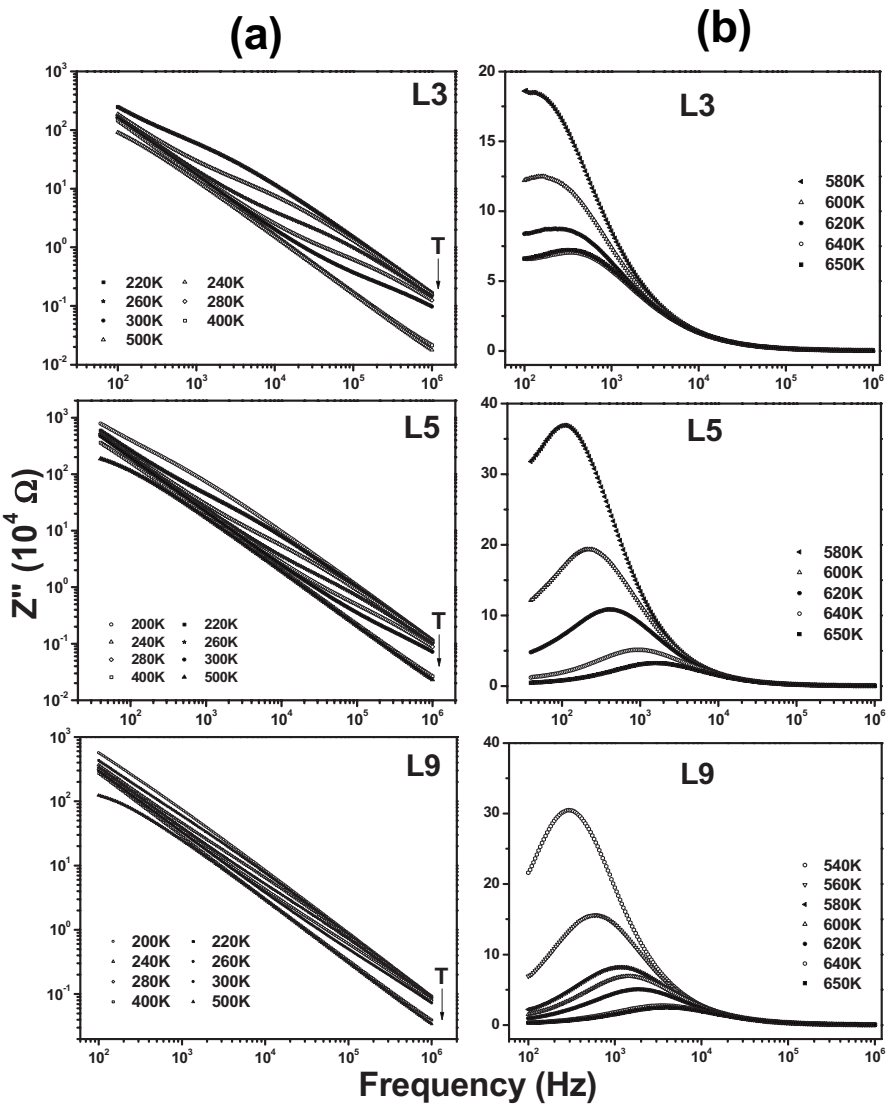

FIG. 4. Frequency dependence of the imaginary part of impedance spectra (Z''): (a) at low temperature, frequency response peaks are mainly due to grain effect, and (b) at elevated temperature (>550 K), low frequency response peaks are mainly due to grain boundary effects (at different temperatures for PZT/CFO multilayer structures).

microstructure and electrical properties, we carried out a detailed temperature dependent impedance spectroscopy analysis in the present multilayers of PZT and CFO; the equivalent circuit used for data analysis consists of two parallel resistor-capacitor (RC) elements connected in series representing the effect of grain and grain boundary [Fig. 3(b)]. The parameters R_g and C_g correspond to the resistance and capacitance of the grain and R_{gb} and C_{gb} are the corresponding quantities for the grain boundary.

B. Impedance analysis

The variation of the imaginary part of impedance (Z'') as a function of frequency is shown in Figs. 4(a) and 4(b) at low and high temperatures, respectively, for L3, L5, and L9 ML configurations. Form Fig. 4(a), in all the ML structures, we observed a weak peak at around 10^4 Hz at 200 K, shifting to higher frequencies with decreased intensity as the temperature increases to 400 K. After 400 K, the peak moves out from our experimental frequency window. When the temperature is increased above 550 K, another strong peak appears in the low frequency range, as shown in Fig. 3(b), for different ML structures; it also moves to higher frequencies with a decrease in intensity as the temperature increases. The intensity of low frequency response peaks decreases rapidly at an elevated temperature; this effect becomes more prominent with the increase in the layers of ML.

Figures 5(a) and 5(b) show the Nyquist plot for L3, L5, and L9 ML structures at 200 and 650 K temperatures, respectively. These MLs exhibit a high impedance value (almost straight line) at low temperature but well-defined semicircle at the temperature >500 K. The extrapolation of these straight lines to a semicircular arc at low temperature is not a precise way to analyze the electrical behavior of ML. From Figs. 5(a) and 5(b), we can observe the magnitude of Z' (at $Z''=0$) decreased with the increase in the number of layers at the constant temperature.

To analyze, the impedance data are usually modeled by an ideal equivalent electrical circuit comprising of resistance (R) and capacitance (C). The equivalent circuit is based on the brick-layer model. The ideal brick-layer model can be represented by Fig. 3(a). We ignore the parallel channel of grain boundary resistance and capacitance. These polycrystalline MLs show that grain and grain boundary impedance

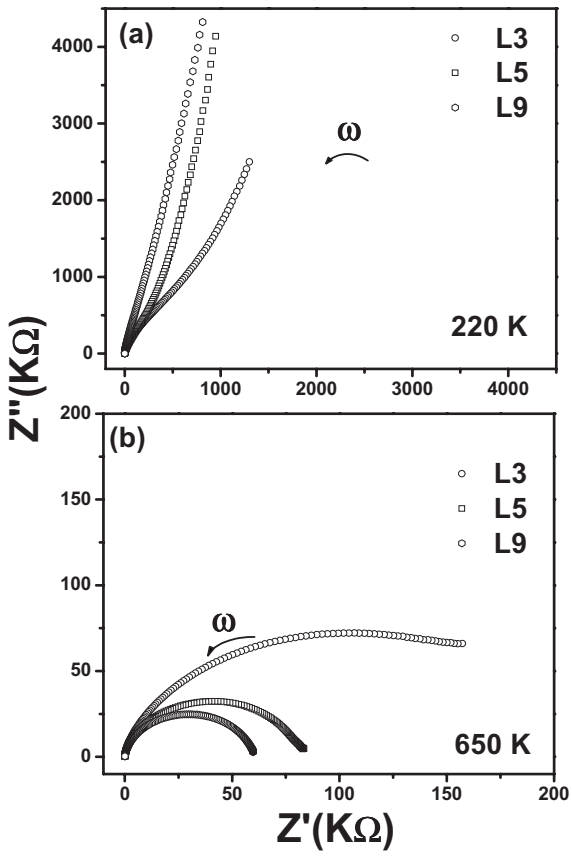

FIG. 5. Complex impedance plane plot (Z'' vs Z') for PZT/CFO ML at (a) 220 K and (b) 650 K.

can be represented by an equivalent circuit given in Fig. 3(b). The circuit consists of series combination of grain and grain boundary elements. The grain circuit consists of parallel combination of grain resistance (R_g) and grain capacitance (C_g), whereas the grain boundary consists of the parallel combination of grain boundary resistance (R_{gb}) and grain boundary capacitance (C_{gb}). The equivalent electrical equation can be represented by

$$Z^* = Z' - jZ'' = \frac{1}{R_g^{-1} + j\omega C_g} + \frac{1}{R_{gb}^{-1} + j\omega C_{gb}}, \tag{6}$$

$$Z' = \frac{R_g}{1 + (\omega R_g C_g)^2} + \frac{R_{gb}}{1 + (\omega R_{gb} C_{gb})^2}, \tag{7}$$

$$Z'' = R_g\left[\frac{\omega R_g C_g}{1 + (\omega R_g C_g)^2}\right] + R_{gb}\left[\frac{\omega R_{gb} C_{gb}}{1 + (\omega R_{gb} C_{gb})^2}\right], \tag{8}$$

$$Z'' = R_{gb}\left[\frac{\omega R_{gb} C_{gb}}{1 + (\omega R_{gb} C_{gb})^2}\right]. \tag{9}$$

As shown in Fig. 4(a), the impedance loss peaks attributed to the grains are so weak that we cannot analyze data by Eq. (8). At elevated temperature (>400 K), the strong impedance loss peak attributed to the grain boundary in the low frequency side appears in the experimental frequency window while grain peaks already moved out. Hence, the magnitude of impedance loss (Z'') can be fitted by an equivalent circuit consisting of parallel combination of C_{gb} and R_{gb} [given in Fig. 3(c)] and can be represented by Eq. (9). In the ideal Debye-type relaxation, the electrical response can be represented by

$$Z^* = \frac{1}{R_{gb}^{-1} + j\omega C_{gb}}. \tag{10}$$

However, in reality, Z'' can be described by using the Cole-Cole equation which is commonly used for polycrystalline materials,

$$Z^* = \frac{R_{gb}}{R_{gb} + (j\omega\tau)^{\alpha}}, \tag{11}$$

where τ is the relaxation time and $\alpha(0 < \alpha \leqslant 1)$ is the parameter used to calculate the deviation from the ideal Debye-type relaxation. We fitted our data with the Debye model; we observed that the response from the grain boundary does not follow the ideal Debye relaxation. The full width at half maxima calculated from impedance loss spectra are greater than 1.141 decade (ideal Debye relaxation) and the deviation parameter less than 1 for different MLs at different temperature indicates the deviation from Debye-type relaxation. The activation energy associated with the grain boundary relaxation process was determined from the frequencies at which the maximal f_p occur using the Arrhenius equation

$$\tau = \tau_0 \exp(-E_a/k_B T), \quad \tau = 1/2\pi f_p, \tag{12}$$

where τ_0 is the prefactor, E_a is the activation energy for the relaxation process, and k_B is the Boltzman constant. From the slopes of the fitted straight lines, we obtain the grain boundary activation energy (E'_{gb}). The E'_{gb} values in the case of L3, L5, and L9 are listed in the Table I. The value of grain boundary activation energy increases with the increase in the

TABLE I. Activation energies and prefactors of the grain (E_g, τ_{0g}) and grain boundary (E_{gb}, τ_{0gb}) relaxation processes determined by fitting the M'' data and average of the stretched exponential parameter (β) for each ML structure E'_{gb} was calculated from Z'' vs f.

Films	E'_{gb} (eV)	E_g (eV)	E_{gb} (eV)	τ_g (s)	τ_{gb} (s)	β_g	β_{gb}
L3	0.515	0.4187	0.5684	$10^{-13.08}$	$10^{-7.81}$	0.435	0.490
L5	1.178	0.3938	1.1438	$10^{-12.63}$	$10^{-12.43}$	0.466	0.596
L9	0.995	0.4168	0.9884	$10^{-12.73}$	$10^{-11.47}$	0.412	0.703

number of layers of ML but it becomes perturbed with the increase in the number of layers. This indicates that more energy is required for the mobility of charge carriers through the grain boundary in L5 and L9 ML structures. The value of activation energy for L9 is little less than L5; this may be due the redistribution of relaxation time after a certain number of layers. The response time decreases with the increase in layers of ML, which implies a small grain boundary resistance for L9, decreasing in grain boundary resistance attributed to the high activation energy in L5 and L9 compared to L3. Later, we will discuss in more detail the activation energy calculated from electrical modulus spectroscopy.

The magnitude of grain boundary resistances was decreased from ~250 kΩ (extrapolation of curve to meet at the *x* axis) (L3) to ~60 kΩ (L9) at 650 K. Since the number of layers increases from L3 to L9, the individual thickness of each PZT or CFO layers decreases, which increases the interdiffusion region with respect to the individual layers. It indicates more grain boundary contribution from the L9 ML. Sketch diagram of the L9 ML structure indicates more grain boundary path compared to the other structure. In reality, at elevated temperature, this path acts like a short circuit for conduction of charge carriers, which drastically reduce the grain boundary resistance.

C. Modulus formalism

We have already observed very weak grain effects in impedance loss spectra compared to grain boundary effects. As we know, smaller capacitance value will dominate in the electric modulus spectra, which magnify the grain effects rendering them easier to analyze. In order to analyze the grain effects, we discussed our results in the context of modulus formalism. The complex modulus plot is shown in Fig. 6 for L3, L5, and L9 ML configurations. The data indicate the presence of two resolved semicircle: the first semicircle represents the capacitive grain boundary effects in low temperature regions and the second one represents the capacitive grain effects at elevated temperature.[11,13]

The common features which we observed in all the MLs are summarized as follows: (i) grain and grain boundary effects fall into two different temperature regions, i.e., low temperature (below 400 K) and high temperature (above 400 K); (ii) well resolved big semicircle from grain effects at low temperature which decreased with the increase of the layers of ML; (iii) when the temperature increased above 400 K, the grain effect moved out, while grain boundary effect entered in the measured frequency range; (iv) the magnitude of grain capacitance increases from L3 to L9 at low temperature (<400 K), while the magnitude of grain boundary capacitance decreases from L3 to L9; (v) grain and grain boundary capacitance are weakly temperature dependent; (vi) the magnitudes of grain boundary capacitance are roughly ten, five, and one to two times greater than the grain capacitance in the case of L3, L5, and L9, respectively.

The imaginary electrical (M'') moduli for L3, L5, and L9 ML thin films as a function of the frequency are shown in Figs. 7(a)–7(c) at low (lower) and high (upper) temperatures, respectively. Similar to the impedance formalism, the response frequency of grain and grain boundary almost fall into two different frequency ranges. The peak position of response frequencies of grain effect shifted (which appear in M'' below 400 K) rapidly toward the higher frequency side with the increase in temperature, while in the case of grain boundary effect, it is confined in the low frequency window. Above ~420 K, the grain boundary peaks start appearing in the studied frequency window as the same grain peaks move out from the frequency window.[11,13]

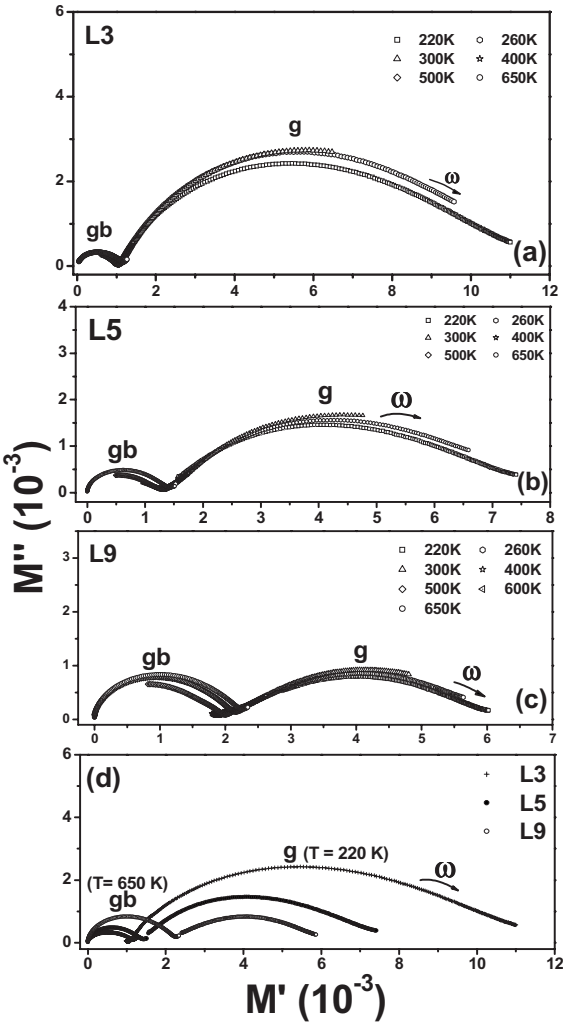

FIG. 6. Complex electric modulus plane plot (M'' vs M') at different temperatures for (a) L3, (b) L5, and (c) L9 PZT/CFO structures. (d) M'' vs M' plot for PC multilayer structures at 220 and 650 K.

The intensities of the grain peaks of the L3 film are about eight times greater than the grain boundary peak, which decreased to 5 and 2 for L5 and L9, respectively, indicating that the grain capacitance (C_g) of multilayers is smaller than the grain boundary capacitance (C_{gb}). These results matched well with the observation from the complex modulus plot. We also observed that the difference in magnitude between C_g and C_{gb} decreases with the increase in the number of layer of ML, which indicates the increase of the interdifussion region between PZT and CFO with increasing

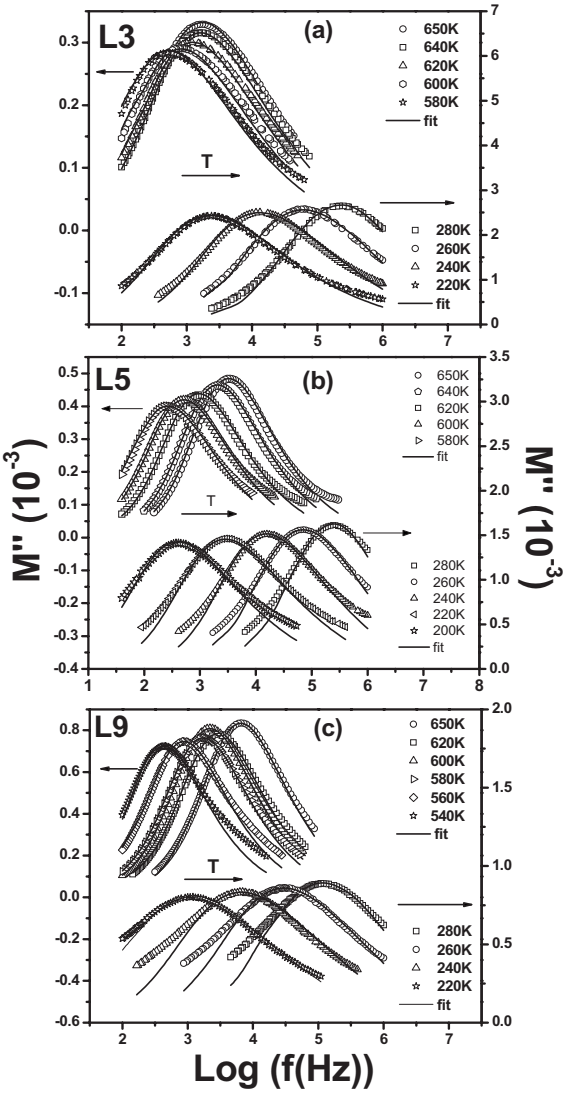

FIG. 7. Frequency dependence of the imaginary part (M'') of electric modulus for (a) L3, (b) L5, and (c) L9 PZT/CFO ML thin films at low (lower) and higher (upper) temperatures, respectively.

number of layers, resulting in a more heterogeneous composite structure.

To explain the above result, we analyzed our data with the complex electrical modulus formalism. The electric modulus $M^*(\omega)$ corresponds to the relaxation of the electric field in the material when the electric field displacement remains constant. The expression for the decay of electric field in time domain can be written as

$$E(t) = E(0) \times \phi(t), \tag{13}$$

where $\phi(t)$ is a macroscopic decay function of the general form

$$\phi(t) = \int_0^\alpha g(\tau) e^{(-t/\tau)\beta} d\tau, \tag{14}$$

where τ is an electric or conductivity relaxation time and $g(\tau)$ is a normalized density function for relaxation times. In the frequency domain, this process may be described by

$$M^*(\omega) \equiv 1/\varepsilon^*(\omega) = M' + iM'', \tag{15}$$

$$M^*(\omega) = M_s \left\{ 1 - \int_0^\alpha \exp(-i\omega t)[-d\phi(t)/dt]dt \right\}, \tag{16}$$

$$= M_s \left\{ \int_0^\alpha g(\tau)[i\omega\tau/(1+i\omega\tau)]d\tau \right\}, \tag{17}$$

where M_s is the high frequency limit of the real part of the electrical modulus.[17,18] The M'' fitting data for each multilayer structure were performed using the known Kohlraush-William-Watt stretched exponential function,[19,20] $\phi(t) = \phi_0 \exp[-(t/\tau)^\beta]$, as the decay function of the electric field within the material, where β is the stretched exponent parameter $(0 < \beta < 1)$ and it characterizes the width of the relaxation time distribution. τ is defined as the most probable relaxation time. The modulus fitting for each multilayer structure was performed using the procedure of Moynihan *et al.*[21] by employing the fitting algorithm described elsewhere.[22] The continuous lines in Fig. 7 are the fitted value of M'', whereas the symbols correspond to the experimental data. The close agreement between the experimental data and the fitting curve is evident from Fig. 7 for L3, L5, and L9 multilayer films.

The stretched exponential parameters β obtained from the fitting were listed in Table I. It was found that it is independent of the temperature and that the distribution of relaxation times is also independent of temperature. For multilayer structures, β_g values are very close; this means that there is no significant difference in the width of the relaxation spectra in the case of the grain relaxation process. In contrast, the value of β_{gb} increased when the number of layers increases; it suggests that the distribution of relaxation time became narrower with increasing number of layer. We correlate our results to the grain boundary conduction at high temperature. It is found that β increases as the interaction among mobile carrier decreases, resulting in the increase in conductivity.[23,24] The results show that β increases linearly with the increase in number of layers in ML, strongly suggesting grain boundary dependent conductivity.

The relaxation time τ resulting from the M'' fits for the low and high temperature response peaks was plotted against the inverse temperature. We found that the fitted τ value at different temperatures was followed by the Arrhenius law. The activation energies of grain and grain boundary calculated from the slopes of the fitted straight lines are given in Table I. The values corresponding to E_{gb} are in good agreement with the value obtained from the Z'' vs f plot (E'_{gb}). The activation energy due to grain effect is similar for all the MLs, indicating that the response time decreases with the similar rate. The value of E'_{gb} increased with the increase in the layers of ML, which indicates the decrease of the grain boundary capacitance, and matched well with the value calculated from modulus loss spectra and observed in impedance loss spectra.

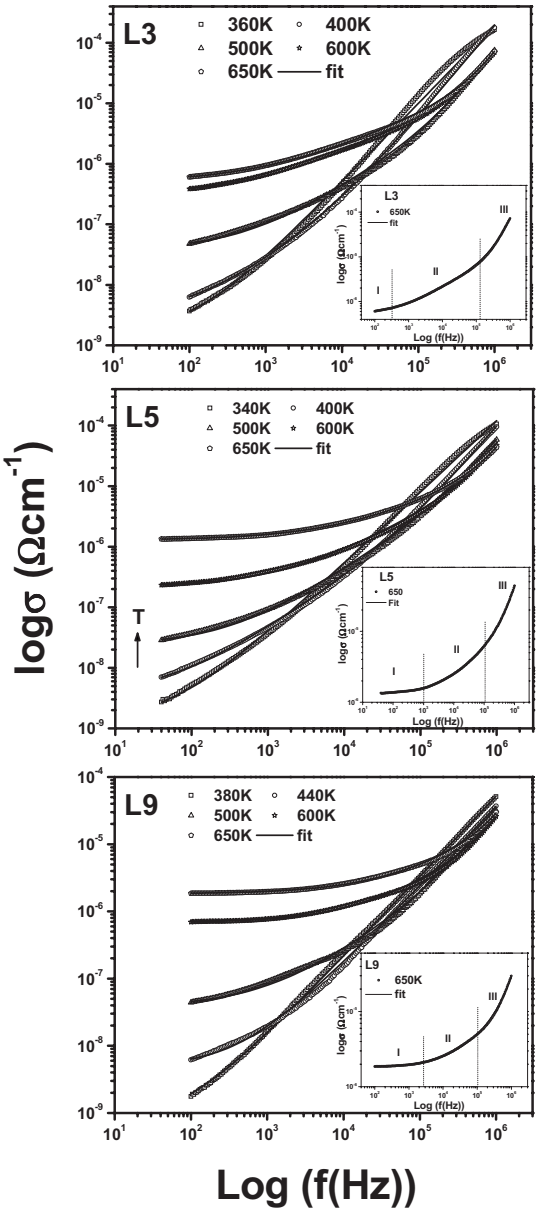

FIG. 8. Frequency dependence plot of the ac conductivity at different temperatures for PZT-CFO multilayer thin film. The double power law fits are shown as continuous lines.

D. ac conductivity analysis

The frequency dependence of conductivity at different temperatures for ML structures is shown in Fig. 8. The conductivity plots of ML thin films possess the following characteristics: (i) dispersion and merging of conductivity spectra at lower and higher frequencies, respectively, with the increase in temperature; (ii) at temperatures below 400 K, the conductivity becomes a strong function of frequency and the dc plateau is unobservable in the available frequency window; (iii) above 400 K, frequency independent conductivity in low frequency regions (<1 kHz), a frequency dependent plateau in midfrequency regions, and frequency dependent conductivity at high frequency regions; (iv) an enhancement of 4–5 orders of frequency independent conductivity with the increase in temperature (from 220 to 625 K), this behavior becomes more prominent with the increase in the number of layers of ML

The above-mentioned observation in conductivity spectra can be explained on the basis of the jump relaxation model and conduction through grain boundaries. The frequency independent plateau at a low frequency for higher temperatures (>620 K) is attributed to the long-range translational motion of ions contributing to dc conductivity (σ_{dc}). The observed frequency independent dc conductivity (higher temperature) was explained by Funke[25] in the jump relaxation model (JRM). According to this model, the conductivity at the low frequency region is associated with the successful hops to its neighborhood vacant site due to the available long time period; such successive jumps result in a long-range translational motion of ions contributing to dc conductivity. At high frequency ($>10^4$ Hz), two competing relaxation processes may be visualized: (i) the jumping ion to jump back to its initial position (correlated forward-backward-forward), i.e., unsuccessful hopping and (ii) the neighborhood ions become relaxed with respect to the ion's position (the ions stay in the new site), i.e., successful hop. The increase in the ratio of successful to unsuccessful hopping results in a more dispersive conductivity at high frequencies. A convenient formalism to investigate the frequency behavior of conductivity at constant temperature in a variety of materials is based on the power relation proposed by Jonscher,[26]

$$\sigma(\omega) = \sigma(0) + A\omega^n, \tag{18}$$

where $\sigma(\omega)$ is the total conductivity, $\sigma(0)$ is the frequency independent conductivity, and the coefficient A and exponent n $(0<n_1<1)$ are temperature and material intrinsic property dependent constants.[27] The term $A\omega^n$ contains the ac dependence and characterizes all dispersion phenomena. The conductivity results in this study for PZT/CFO multilayers do not follow this relation. From the insets in Fig. 8, it is clear that after the dc plateau (region I), as frequencies increase, two dispersion regions appear; the low frequency dispersion is associated with the grain boundary (large capacitance value) (region II) and the high frequency one with grains (smaller capacitance value) (region III).

Applying the JRM (the frequency dependence of the conductivity of the ML thin films), the data have been fitted to a double power law,[25,28]

$$\sigma(\omega) = \sigma(0) + A_1\omega^{n_1} + A_2\omega^{n_2}, \tag{19}$$

to describe the different contributions to conductivity, which means that at very low frequencies, an almost frequency independent region is present, followed by two dispersive regions. The term $\sigma(0)$ (region I) corresponding to the translation hopping gives the long-range electrical transport (i.e., dc conductivity) in the long time limit. The second one $A_1\omega^{n_1}$ was assigned to region II; the exponent $0<n_1<1$ characterizes the low frequency region and corresponds to the translational hopping motion (short-range hopping). Whereas the one at high frequencies $A_2\omega^{n_2}$ is associated to region III, the exponent $0<n_2<2$ corresponds to a localized or reorientational hopping motion.[25] The conductivity behavior of L3,

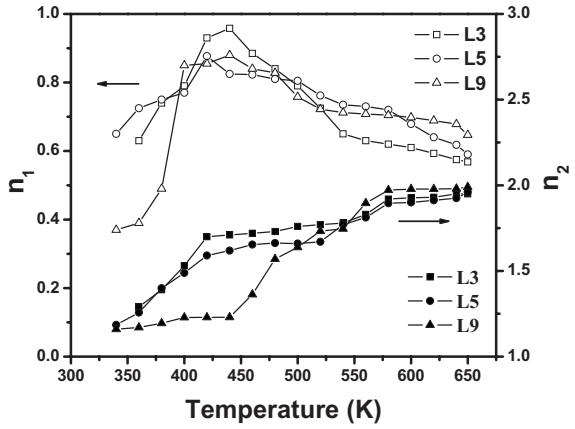

FIG. 9. Variation of double power law exponents (n_1, n_2) as a function of temperature of PZT-CFO multilayer structures.

L5, and L9 MLs fitted with the double power law by nonlinear regression analysis is shown in the Fig. 7 (solid lines) at different temperatures.

Figure 9 shows n_1 and n_2 values as functions of temperature obtained from the fitted data for all the ML structures. The values for n_1 and n_2 were found to vary between 0.35–0.95 and 1.1–1.9, respectively. In the temperature range from 400 to 500 K, n_1 vs T shows a peak and n_2 vs T shows a steplike peak. This temperature corresponds to the onset of the crossover from the grain contribution to the grain boundary contribution well supported by frequency and temperature dependent impedance and modulus plots (Figs. 4 and 7). Since different hopping mechanisms have been reported by different researchers and these mechanisms predict different temperature and frequency dependencies of the exponent n, in the case of small polaron hopping, n increases with temperature, while for a large polaron hopping mechanism, n decreases with increasing temperature.[28,29] From Fig. 9, the values of n_1 are less than 1, and also n_1 increases below 450 K and decreases above 450 K; hence, the conduction arises in region II (inset Fig. 8) due to the short-range translation hopping assisted by both small polaron ($T<450$ K) and large polaron ($T>450$ K) hopping mechanisms. In the case of n_2, values are found varying between 1 and 2 and increase with increasing temperature; hence, the conduction could be attributed to the localized orientation hopping (hopping of electron back and forth between two charge defects and the presence of induced or permanent dipoles) assisted by small polaron mechanism.[28–32]

In the present ML thin films, the high frequency localized orientation hopping may be attributed to the formation of dipoles; the coexistence of the low dielectric constant phase (CFO) with the high dielectric constant phase (PZT) can influence the piling charges at the interface and hence the Maxwell-Wagner (MW)-type polarization. The MW dispersion is caused by interfacial polarization due to spatial variants of the conductivity of the material.[33–35]

V. CONCLUSIONS

We have investigated frequency and temperature dependencies of the impedance, modulus, and conductivity spectra of PZT-CFO multilayer structures with three, five, and nine layers. STEM line scale has been used across the ML structure to check its chemical purity. Diffraction patterns showed clear PZT and CFO crystals near the interface and interior of the ML structure. We found that ML deposition has interdiffusion near the interface, which makes it inhomogeneous, and this behavior becomes prominent with the increase in the number of layers. Micro-Raman spectra indicate no chemical impurity in the ML structure. We observed two separate conduction processes in impedance and modulus spectra attributed to grain and grain boundary effects. We also observed that there is a deviation from the Debye-type relaxation in the impedance loss spectra. The stretching exponent parameter β_{gb}, calculated from modulus spectra, increased linearly with the increase in the number of layers in ML and it suggested the grain boundary dependent conductivity at elevated temperatures. The conductivity spectra obey well the double power law, indicating different contributions to the conductivity; the low frequency conductivity is due to the long-range translational hopping, the midfrequency conductivity is due to the short-range translational hopping, and the high frequency conductivity is due to the localized or reorientational hopping motion. We also observed MW dispersion caused by the interfacial polarization due to spatial variants of the conductivity of the material.

ACKNOWLEDGMENTS

This work was supported in part by DoD-W911NF-06-1-0030 and W911NF-06-1-0183 grants. The authors thank Oscar Resto for his help with the TEM measurements.

*Corresponding author; FAX: 787-764-2571; rkatiyar@uprrp.edu

[1] J. F. Scott, Science **315**, 954 (2007).
[2] N. A. Spaldin and M. Fiebig, Science **309**, 391 (2005).
[3] K. S. Chang, M. A. Aronova, C. L. Lin, M. Murakami, M. H. Yu, J. H. Simpers, O. O. Famodu, S. Y. Lee, R. Ramesh, M. Wuttig, I. Takeuchi, C. Gao, and L. A. Bendersky, Appl. Phys. Lett. **84**, 3091 (2004).
[4] J. P. Zhou, H. He, Z. Shi, and C. W. Nan, Appl. Phys. Lett. **88**, 013111 (2006).
[5] P. Murugavel, M. P. Singh, W. Prellier, B. Mercey, Ch. Simon, and B. Raveau, J. Appl. Phys. **97**, 103914 (2005).
[6] H. Zheng, J. Wang, S. E. Lofland, Z. Ma, L. M. Ardabili, T. Zhao, L. S. Riba, S. R. Shinde, S. B. Ogale, F. Bai, D. Viehland, Y. Jia, D. G. Schlom, M. Wuttig, A. Roytburd, and R. Ramesh, Science **303**, 661 (2004).
[7] N. Ortega, P. Bhattacharya, R. S. Katiyar, P. Dutta, A. Manivannan, M. S. Seehra, I. Takeuchi, and S. B. Majumder, J. Appl. Phys. **100**, 126105 (2006).

[8] O. Raymond, R. Font, N. Suarez-Almodovar, J. Portelles, and J. M. Siqueiros, J. Appl. Phys. **97**, 084108 (2005).
[9] K. Srinivas, P. Sarah, and S. V. Suryanarayana, Bull. Mater. Sci. **26**, 274 (2003).
[10] D. C. Sinclair, T. B. Adams, F. D. Morrison, and A. R. West, Appl. Phys. Lett. **80**, 2153 (2002).
[11] Jianjun Liu, Chun-Guan Duan, Wei Guo Yin, W. N. Mei, R. W. Smith, and J. R. Hardy, Phys. Rev. B **70**, 144106 (2004).
[12] Jianjun Liu, Chun-Guan Duan, W. N. Mei, R. W. Smith, and J. R. Hardy, J. Appl. Phys. **98**, 093703 (2005).
[13] P. Victor, S. Bhattacharyya, and S. B. Krupanidhy, J. Appl. Phys. **94**, 5135 (2003).
[14] G. Catalan, Appl. Phys. Lett. **88**, 102902 (2006); G. Catalan and J. F. Scott, Nature (London) **448**, E4-E5 (2007).
[15] G. Catalan, D. O'Neill, R. M. Bowman, and J. M. Gregg, Appl. Phys. Lett. **77**, 3078 (2000).
[16] N. Ortega, Ashok Kumar, R. S. Katiyar, and J. F. Scott, Appl. Phys. Lett. **91**, 102902 (2007).
[17] P. B. Macedo, C. T. Moynihan, and R. Bose, Phys. Chem. Glasses **13**, 171 (1972).
[18] V. Provenzano, L. P. Boesch, V. Volterra, P. B. Macedo, and C. T. Moynihan, J. Am. Ceram. Soc. **55**, 492 (1972).
[19] R. Kohlrausch, Ann. Phys. **12**, 393 (1847).
[20] G. Williams and D. C. Watts, Trans. Faraday Soc. **66**, 80 (1970).
[21] C. T. Moynihan, L. P. Boesch, and N. L. Laberge, Phys. Chem. Glasses **14**, 122 (1973).
[22] N. Baskaran, J. Appl. Phys. **92**, 825 (2002).
[23] H. K. Patel and S. W. Martin, Phys. Rev. B **45**, 10292 (1992).
[24] K. L. Ngai, G. N. Greaves, and C. T. Moynihan, Phys. Rev. Lett. **80**, 1018 (1998).
[25] K. Funke, Prog. Solid State Chem. **22**, 111 (1993).
[26] A. K. Jonscher, Nature (London) **264**, 673 (1977).
[27] A. P. Almond, A. R. West, and R. J. Grant, Solid State Commun. **44**, 277 (1982).
[28] A. Pelaiz-Barramco, M. P. Gutierrez-Amador, A. Huanosta, and R. Valenzuela, Appl. Phys. Lett. **73**, 2039 (1998).
[29] A. A. A. Youssef, Z. Naturforsch., A: Phys. Sci. **57**, 263 (2002).
[30] A. R. James, Chandra Prakash, and G. Prasad, J. Phys. D **39**, 1635 (2006).
[31] S. Mahbood, G. Prasad, and G. S. Kumar, Bull. Mater. Sci. **29**, 347 (2006).
[32] J. Ross Macdonald, J. Non-Cryst. Solids **210**, 70 (1997).
[33] Reji Thomas, V. K. Varadan, S. Komarneni, and D. C. Dube, J. Appl. Phys. **90**, 1480 (2001).
[34] M. Kitao, Jpn. J. Appl. Phys. **11**, 1472 (1972).
[35] Upadhyay Shail, Sahu Ashok Kumar, Devender Kumar, and Om Parkash, J. Appl. Phys. **84**, 828 (1998).